Journal of Engineering and Technology for Industrial Applications

ITEGAM-JETIA

Manaus, v.12 n.58, p. 342-355. March/April, 2026.
DOI: https://doi.org/10.5935/jetia. v12i58.3067

ISSN ONLINE: 2447-0228

RESEARCH ARTICLE OPEN ACCESS

A DEVELOPMENT OF FUZZY-PID CONTROLLER APPLIED ON AN AUTONOMOUS SURFACE VEHICLE

Thien M. Tran[*1] and Tien V. Tran[2]

[1, 2]Department of Mechatronics, Faculty of Mechanical Engineering, Ho Chi Minh City University of Technology and Engineering (HCM-UTE), Ho Chi Minh City (700000), Vietnam

[1]http://orcid.org/0000-0003-3465-5905, [2]http://orcid.org/0009-0008-8993-9634

Email: [*]thientm@hcmute.edu.vn

ARTICLE INFO

Article History
Received: December 6, 2025
Reviewed: January 7, 2026
Accepted: January 14, 2026
Published: March 31, 2026

Keywords:
Autonomous Surface Vehicle (ASV),
nonlinear dynamics,
fuzzy-PID control,
trajectory tracking,
marine cybernetics

ABSTRACT

Precise trajectory tracking remains a significant challenge for Autonomous Surface Vehicles (ASVs) due to their inherent nonlinear and strongly coupled surge-sway-yaw dynamics, which are often exacerbated by environmental disturbances. This study aims to enhance the trajectory tracking performance and robustness of an ASV by developing an adaptive Fuzzy-PID controller and comparing its efficacy against a conventional Proportional-Integral-Derivative (PID) controller. A comprehensive 3 degree of freedom (DoF) mathematical model of the ASV is derived using the Fossen modeling framework, incorporating rigid-body kinetics, hydrodynamics, and environmental disturbances. A novel single-loop Fuzzy-PID control architecture is then proposed, wherein a Mamdani-type fuzzy inference system dynamically tunes the PID gains online based on the tracking error and its derivative. The performance of the proposed controller is rigorously evaluated against a classical PID controller through simulations involving circular and lemniscate trajectories, which are designed to stress the system's dynamic coupling. The simulation results demonstrate the superior performance of the Fuzzy-PID controller. It achieves a substantial reduction in steady-state heading bias up to 46% in Root Mean Square Error (RMSE) and 64% in Integral Absolute Error (IAE) for the circular trajectory compared to the conventional PID. Furthermore, the proposed controller delivers smoother control signals, faster settling times, and improved robustness under strong dynamic coupling and external perturbations. The proposed Fuzzy-PID controller provides a significant improvement in tracking accuracy and adaptability over the conventional PID controller. It offers an efficient and practical solution for the autonomous guidance and control of small-scale surface vehicles, effectively handling nonlinearities and coupled dynamics. Future work will focus on hardware-in-the-loop validation and incorporation of advanced disturbance observers.

I. INTRODUCTION

Autonomous Surface Vehicles (ASVs) have undergone a significant transformation, evolving from experimental testbeds into indispensable workhorses for a wide range of maritime applications. Their roles now encompass persistent oceanographic monitoring, environmental sensing, offshore infrastructure inspection, and cooperative missions alongside aerial and underwater robots [1], [2]. The operational effectiveness of these platforms in such complex tasks is fundamentally dependent on their ability to execute precise and robust trajectory tracking. As Fossen [3] emphasizes, this capability is not only crucial for high-speed route following but also serves as a foundational building block for more advanced maneuvers such as dynamic positioning (DP) and coordinated multi-vehicle formation control [4]. The core challenge in achieving this precision lies in the inherent complexity of ASV dynamics. The horizontal-plane motion of an ASV is governed by a highly nonlinear, strongly coupled surge-sway-yaw system.

Standard marine control models, as detailed in [1], [3], [5], [6] incorporate rigid-body inertia, hydrodynamic added mass, Coriolis and centripetal forces, and complex damping effects that combine linear and quadratic components. These dynamics are further complicated by unmodeled hydrodynamic phenomena [6-8] and persistent environmental disturbances from wind, waves, and currents [3], [6]. The resultant cross-coupling, particularly between sway and yaw, means that a control action in one degree of freedom can induce significant deviations in others, making the design of a high-performance tracking controller a non-trivial endeavor. In the face of these challenges, the PID controller has remained a cornerstone of marine control systems due to its straightforward structure, ease of implementation, and generally acceptable performance for a wide range of operating conditions [9].

Its widespread use in commercial autopilots and many research ASVs is a testament to its practicality. However, [9] and [10] point out, the performance of a fixed-gain PID controller is highly dependent on careful tuning and is often compromised when confronted with the system's full nonlinearity, strong coupling, and time-varying environmental disturbances. Its lack of adaptability can lead to significant tracking errors, especially during transient maneuvers or when tracking trajectories with varying curvature. To address these limitations, numerous optimization-based and robust control strategies have been proposed in recent years. Rather than discarding the PID structure entirely, [8] developed a Robust and Optimal PID controller. In this approach, the PID gains are optimized using the Successive Loop Closure technique in conjunction with optimization algorithms.

This method ensures vessel stability even in the presence of hydrodynamic model inaccuracies. Furthermore, [11] proposed a Safety-Certified Parallel Model Predictive Control (MPC), which achieves high trajectory tracking accuracy by leveraging its capability to predict future system states. However, a significant drawback of this method is its high computational burden, necessitating high-performance processing hardware and resulting in elevated implementation costs. Another approach aimed at reducing reliance on accurate physical models was introduced by [2], utilizing a combination of Time Delay Estimation (TDE) and Sliding Mode Control (SMC).

This strategy effectively compensates for disturbances and uncertainties, particularly when hydrodynamic parameters are difficult to identify precisely.Additionally, the integration of intelligent control techniques, such as Fuzzy Logic or Neural Networks, has proven effective in handling the inherent nonlinearity and uncertainties of ASV systems. By [4] successfully applied a Fuzzy-PID controller to formation control problems, employing a fuzzy system to automatically tune PID gains based on position and heading errors. Their results demonstrated that this method significantly mitigates the zig-zag heading oscillations often observed with traditional PID controllers. A notable advancement in this field is the development of Hybrid Intelligent Systems. In turn [12] proposed a method combining

Dynamic Inversion with Fuzzy Logic, demonstrating superior model error compensation capabilities compared to conventional adaptive methods. Most recently, [13] applied an Adaptive Neuro-Fuzzy Inference System (ANFIS) to the course-keeping problem, achieving a remarkably low RMSE of approximately 1.6%. Collectively, these studies suggest that combining the simple PID structure with intelligent control techniques, such as Fuzzy Logic, offers an effective balance between control performance and computational cost. This approach is particularly suitable for ASV systems operating in complex and uncertain environments. Fuzzy logic, in particular, offers a robust framework for handling system uncertainty and nonlinearity without requiring an explicit mathematical model of all dynamic intricacies.

By encoding expert knowledge into a set of linguistic rules, a fuzzy inference system can dynamically adjust control parameters in real-time, thereby enhancing robustness and adaptability. Building upon this foundation, this paper presents the design and analysis of a single-loop Fuzzy-PID controller for the trajectory tracking of an ASV. The proposed controller retains the operational simplicity of a standard PID but incorporates a fuzzy logic subsystem that continuously adapts the proportional, integral, and derivative gains based on the instantaneous tracking error and its rate of change. This adaptive mechanism allows the controller to respond more effectively to the strongly coupled dynamics and nonlinearities inherent in the ASV's 3-DoF model.

The core objective of this work is to conduct a rigorous, like-for-like comparative analysis to quantify the performance benefits of this fuzzy augmentation over a conventional PID controller, especially when tracking trajectories that explicitly stress the surge-sway-yaw coupling. To validate the proposed approach, extensive simulations were conducted under demanding scenarios, including circular and lemniscate trajectories. The results demonstrate that the Fuzzy-PID controller significantly outperforms the conventional PID controller. Notably, it achieves a substantial reduction in steady-state heading bias during circular tracking and delivers smoother, more accurate path-following with faster settling times in the complex lemniscate maneuver, confirming its superior adaptability and robustness. The main contributions of this research are threefold:

First, a comprehensive 3-DoF mathematical model of the ASV is derived in a vectorial form, adhering to the standard Fossen modeling framework. This model systematically incorporates rigid-body kinetics, hydrodynamics, and environmental disturbances. Second, a novel Fuzzy-PID control architecture featuring a Mamdani-type fuzzy inference system is developed. In this system, the tracking error and its derivative are utilized as inputs to dynamically tune the PID gains online, thereby enhancing the controller's adaptability and robustness. Third, an extensive simulation-based evaluation is conducted under two distinct reference trajectories-circular and lemniscate which are designed to progressively exacerbate dynamic coupling and challenge controller performance. The comparative analysis employs quantitative metrics such as RMSE and IAE to conclusively demonstrate the superior tracking accuracy, improved transient response, and reduced steady-state error achieved by the proposed Fuzzy-PID controller.

It is important to note that this study focuses on establishing the core efficacy of the control architecture. Therefore, to isolate the controller's performance from complex environmental interactions, the simulations are conducted in calm water conditions without explicit modeling of wind, wave, or current spectra. The incorporation of validated environmental models and disturbance observers is a critical direction for future work. The remainder of this paper is structured as follows. Section II details the derivation of the 3-DoF mathematical model for the ASV. Section III elaborates on the design of both the conventional PID and the proposed Fuzzy-PID controller. Section IV presents the simulation setup, results, and a comprehensive discussion of the findings. Finally, Section V concludes the paper by summarizing the key outcomes and outlining potential avenues for future research.

II. MATHEMATICAL MODELING OF AN AUTONOMOUS VEHICLE

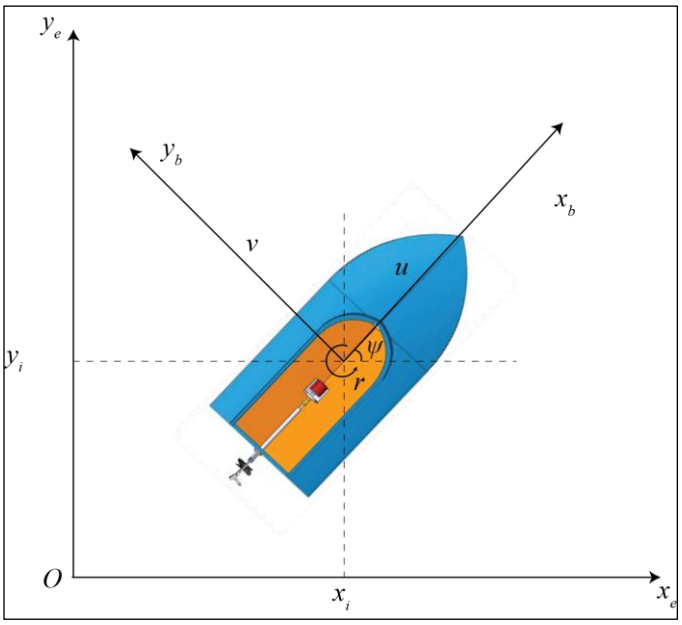

Figure 1: Coordinate System.
Source: Authors, (2026).

The motion of the ASV is described using two reference frames: the earth-fixed inertial frame (NED) and the body-fixed frame attached to the ASV [1], [3]. The kinematic relationship between these frames is expressed as:

$$\dot{\boldsymbol{\eta}} = \mathbf{J}(\psi)\mathbf{v} \tag{1}$$

where: $\boldsymbol{\eta} = [x \quad y \quad \psi]^T$ denotes the earth-fixed position and heading, $\mathbf{v} = [u \quad v \quad r]^T$ denotes the body-fixed linear and angular velocities, and $\mathbf{J}(\psi)$ is the Jacobian rotation matrix following the Euler angle:

$$\mathbf{J}(\psi) = \mathbf{R}_{\mathbf{Z}}(\psi) = \begin{bmatrix} c\psi & -s\psi & 0 \\ s\psi & c\psi & 0 \\ 0 & 0 & 1 \end{bmatrix} \tag{2}$$

Where $c\cdot = \cos(\cdot)$, $s\cdot = \sin(\cdot)$ and the Jacobian $\mathbf{J}(\psi)$ transforms the surge, sway, and yaw rate expressed in the body-fixed frame into global motion variables. The matrix $\mathbf{J}(\psi)$ is orthogonal $\left(\mathbf{J}(\psi)\mathbf{J}^{\mathbf{T}}(\psi) = \mathbf{I}\right)$, with determinant equal to 1, representing a pure rotation without scaling. This kinematic mapping is fundamental in trajectory tracking and path-following control of ASVs. The dynamic model of an ASV [1], [3], [5] is obtained by applying Newton-Euler equations in the horizontal plane. It can be expressed in compact form as:

$$\mathbf{M}\dot{\mathbf{v}} + \mathbf{C}(\mathbf{v})\mathbf{v} + \mathbf{D}(\mathbf{v})\mathbf{v} = \boldsymbol{\tau} + \boldsymbol{\omega}(t) \tag{3}$$

The terms are defined as follows:

- $\mathbf{M} = \mathbf{M}_{\mathbf{RB}} + \mathbf{M}_{\mathbf{A}}$ is the total inertia matrix consisting of the rigid-body inertia and added mass. For an ASV with mass m, yaw inertia I_Z and center of gravity offset x_G,

$$\mathbf{M}_{\mathbf{RB}} = \begin{bmatrix} m & 0 & 0 \\ 0 & m & mx_G \\ 0 & mx_G & I_z \end{bmatrix} \tag{4}$$

$$\mathbf{M}_{\mathbf{A}} = -\begin{bmatrix} X_{\dot{u}} & 0 & 0 \\ 0 & Y_{\dot{v}} & Y_{\dot{r}} \\ 0 & N_{\dot{v}} & N_{\dot{r}} \end{bmatrix} \tag{5}$$

where: $\mathbf{X}_{\dot{\mathbf{u}}} = \frac{\partial \mathbf{X}}{\partial \dot{u}}, \mathbf{Y}_{\dot{\mathbf{v}}} = \frac{\partial \mathbf{Y}}{\partial \dot{v}}, \mathbf{Y}_{\dot{\mathbf{r}}} = \frac{\partial \mathbf{Y}}{\partial \dot{r}}, \mathbf{N}_{\dot{\mathbf{v}}} = \frac{\partial \mathbf{N}}{\partial \dot{v}}, \mathbf{N}_{\dot{\mathbf{r}}} = \frac{\partial \mathbf{N}}{\partial \dot{r}}$ are hydrodynamic derivatives obtained from towing [5].

- $\mathbf{C}(\mathbf{v}) = \mathbf{C}_{\mathbf{RB}} + \mathbf{C}_{\mathbf{A}}$ is the Coriolis-centripetal matrix. For the rigid-body part,

$$\mathbf{C}_{\mathbf{RB}} = \begin{bmatrix} 0 & 0 & -m(x_G r + v) \\ 0 & 0 & mu \\ 0 & -mu & 0 \end{bmatrix} \tag{6}$$

$$\mathbf{C}_{\mathbf{A}} = \begin{bmatrix} 0 & 0 & -Y_{\dot{v}} v - \frac{Y_{\dot{r}} + N_{\dot{v}}}{2} r \\ 0 & 0 & X_{\dot{u}} u \\ Y_{\dot{v}} v + \frac{Y_{\dot{r}} + N_{\dot{v}}}{2} r & -X_{\dot{u}} u & 0 \end{bmatrix} \tag{7}$$

- $\mathbf{D}(\mathbf{v}) = \mathbf{D}_{\mathbf{L}}(\mathbf{v}) + \mathbf{D}_{\mathbf{NL}}(\mathbf{v})$ represents linear and nonlinear hydrodynamic damping forces, where:

$$\mathbf{D}_{\mathbf{L}}(\mathbf{v}) = \begin{bmatrix} X_u & 0 & 0 \\ 0 & Y_v & Y_r \\ 0 & N_v & N_r \end{bmatrix} \tag{8}$$

$$\mathbf{D}_{\mathbf{NL}}(\mathbf{v}) = -\begin{bmatrix} X_{|u|u} u & 0 & 0 \\ 0 & Y_{|v|v} v - Y_{|r|r} r & Y_{|v|r} v - Y_{|r|r} r \\ 0 & N_{|v|v} v - N_{|r|r} r & N_{|v|r} v - N_{|r|r} r \end{bmatrix} \tag{9}$$

Here, the linear damping coefficients consist of X_u (surge drag), Y_v (sway drag), Y_r (sway force from yaw rate), N_v (yaw moment from sway velocity), and N_r (yaw moment from yaw rate). The nonlinear damping $Y_{|v|v}$ and $N_{|v|v}$ denote quadratic drag in sway velocity, while $Y_{|r|r}$ and $N_{|r|r}$ represent quadratic drag in yaw rate. The term $Y_{|v|r}$, $Y_{|r|v}$, $N_{|v|r}$, $N_{|r|v}$ describe nonlinear coupling effects between sway velocity and yaw rate. The control vector input is made up of surge force, sway force and yaw torque are given by the following equation:

$$\boldsymbol{\tau} = \begin{bmatrix} \tau_x & \tau_y & \tau_\psi \end{bmatrix}^T \tag{10}$$

Enviromental disturbances, the low-frequency disturbance vector is denoted as:

$$\boldsymbol{\omega}(t) = \begin{bmatrix} \omega_x(t) & \omega_y(t) & \omega_\psi(t) \end{bmatrix} \tag{11}$$

In this study, $\boldsymbol{\omega}(t)$ is regarded as a generalized disturbance input without explicitly modeling the detailed dynamics of wind, waves, and currents. This assumption simplifies the simulation model while still allowing the controller performance to be evaluated under external perturbations. It represents surge, sway, and yaw disturbances in the earth-fixed frame. For use in the dynamic model, the disturbance must be transformed into the body-fixed coordinates according to:

$$\boldsymbol{\tau}_{\mathbf{d}} = \left[\mathbf{R}_{\mathbf{z}}(\psi)\right]^T \boldsymbol{\omega}(t) = \begin{bmatrix} \omega_x \mathrm{c}\psi + \omega_x \mathrm{s}\psi \\ -\omega_y \mathrm{s}\psi + \omega_y \mathrm{c}\psi \\ \omega_\psi \end{bmatrix} \tag{12}$$

Here, $\boldsymbol{\tau}_{\mathbf{d}}$ represents the surge and sway disturbance forces, and the yaw disturbance moment. The combined horizontal-plane velocity is expressed as:

$$V = \sqrt{u^2 + v^2} \tag{13}$$

III. DESIGN CONTROLLER

III.1 FUZZY-PID CONTROLLER

A single-loop Fuzzy-PID architecture is employed in which the fuzzy inference system receives the position error $\mathbf{e}(t)$ and its time derivative $\dot{\mathbf{e}}(t)$, subsequently outputting incremental corrections $\Delta\mathbf{K}_\mathbf{p}, \Delta\mathbf{K}_\mathbf{i}, \Delta\mathbf{K}_\mathbf{d}$ that retune the baseline PID online. This fuzzy block consists of normalization, inference, and de-normalization stages. Such a design choice capitalizes on the capability of fuzzy rules to encode expert knowledge regarding coupled surge, sway, and yaw interactions, while maintaining the simplicity of a PID controller that is widely utilized in marine applications. To ensure practical robustness, the baseline PID incorporates anti-windup mechanisms and bandwidth-limited derivative filtering, which help to prevent integrator windup and mitigate noise amplification [14], [15]. The Fuzzy-PID controller combines the conventional PID structure with fuzzy logic to improve adaptability and robustness. The control input is given by:

$$\mathbf{u}(t) = \left(\mathbf{K}_\mathbf{p} + \Delta\mathbf{K}_\mathbf{p}\right)\mathbf{e}(t) + \left(\mathbf{K}_\mathbf{i} + \Delta\mathbf{K}_\mathbf{i}\right)\int_0^t \mathbf{e}(t)dt + \left(\mathbf{K}_\mathbf{d} + \Delta\mathbf{K}_\mathbf{d}\right)\dot{\mathbf{e}}(t) \tag{14}$$

Where $\mathbf{e}(t)$ denotes the tracking error, and $\Delta\mathbf{K}_\mathbf{p}, \Delta\mathbf{K}_\mathbf{i}, \Delta\mathbf{K}_\mathbf{d}$ are adaptive corrections provided by the fuzzy inference system. The fuzzy system takes the error $\mathbf{e}(t)$ and its derivative $\dot{\mathbf{e}}(t)$ as inputs. Each input is described by a set of linguistic variables such as Negative Big (NB), Negative Medium (NM), Zero (ZO), Positive Medium (PM), and Positive Big (PB) [16]. The outputs of the fuzzy system are the adjustments $\Delta\mathbf{K}_\mathbf{p}, \Delta\mathbf{K}_\mathbf{i}, \Delta\mathbf{K}_\mathbf{d}$ which dynamically modify the PID gains as:

$$\mathbf{K}_\mathbf{p} = \mathbf{K}_{\mathbf{p0}} + \Delta\mathbf{K}_\mathbf{p}, \quad \mathbf{K}_\mathbf{i} = \mathbf{K}_{\mathbf{i0}} + \Delta\mathbf{K}_\mathbf{i}, \quad \mathbf{K}_\mathbf{d} = \mathbf{K}_{\mathbf{d0}} + \Delta\mathbf{K}_\mathbf{d}$$

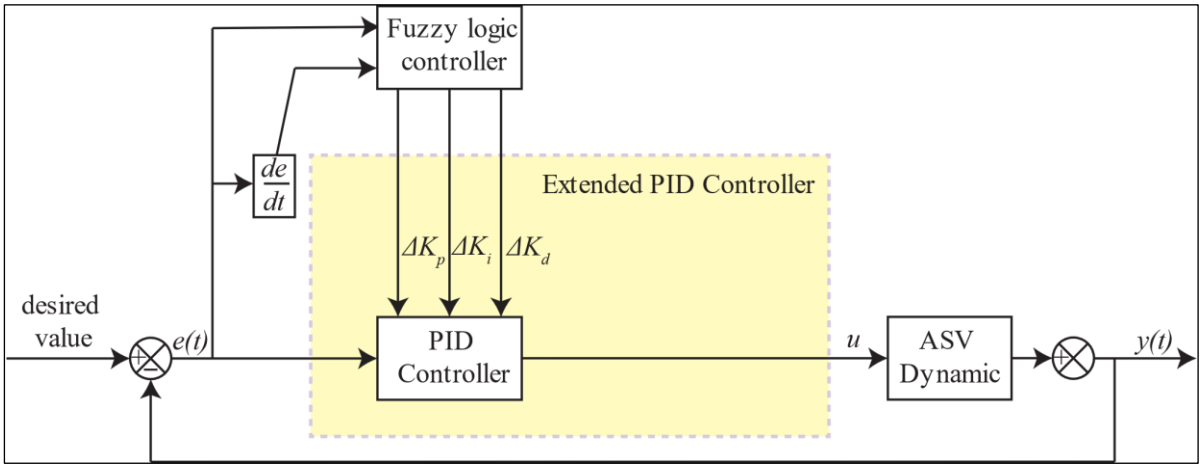

Figure 2: Structure of Fuzzy-PID controller.
Source: Authors, (2026).

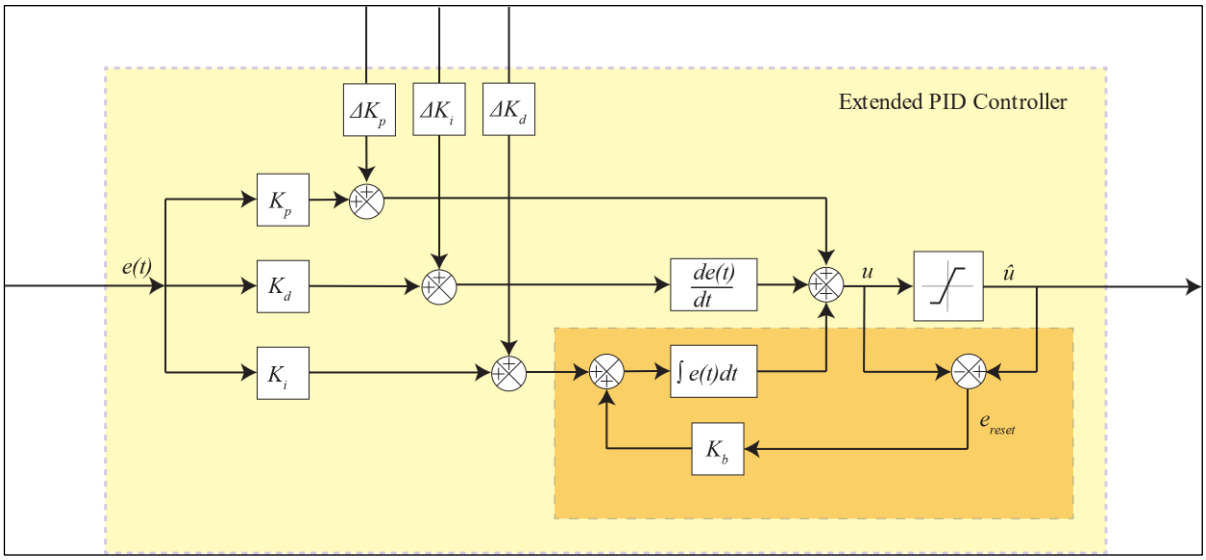

Figure 3: Block diagram of an Extended PID controller.
Source: Authors, (2026).

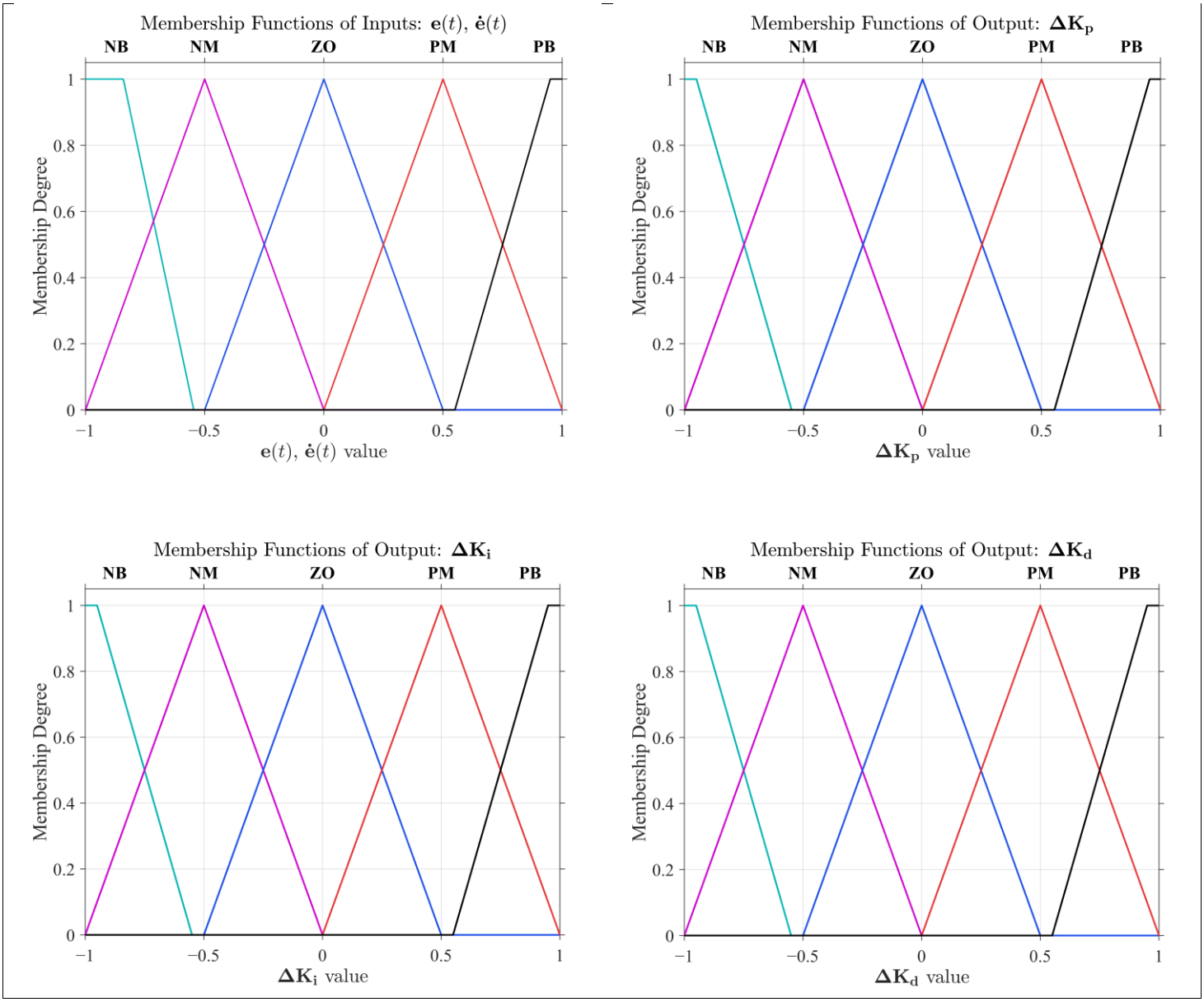

Figure 4: Input and Three Output Membership Functions of the Fuzzy Logic System.
Source: Authors, (2026).

Mamdani fuzzy systems employ rule bases of the form IF (error is NB) AND (error rate is NM) THEN (output is PB)... providing a human-interpretable control structure [15], [16]. The fuzzy control rules are formulated in the form *"IF error* $\mathbf{e}(t)$ *is ... AND error change* $\dot{\mathbf{e}}(t)$ *is ... THEN* $\Delta\mathbf{K}$ *"*. Based on expert knowledge and simulation tuning, the final rule bases for $\Delta\mathbf{K_p}, \Delta\mathbf{K_i}, \Delta\mathbf{K_d}$ were established. These rules are shown in below table:

Table 1: Fuzzy control rules table of scale coefficient.

$\Delta\mathbf{K_p}$		$\mathbf{e}(t)$				
		NB	NM	ZO	PM	PB
$\mathbf{e}(t)$	NB	PB	PB	PB	PB	PB
	NM	PM	PM	PM	PM	PM
	ZO	PM	PM	ZO	PM	PM
	PM	NM	NM	NM	NM	NM
	PB	NB	NB	NB	NB	NB

Source: Authors, (2026).

Table 2: Fuzzy control rules table of integral coefficient.

$\Delta \mathbf{K_i}$		$\mathbf{e}(t)$				
		NB	NM	ZO	PM	PB
$\dot{\mathbf{e}}(t)$	NB	NB	NM	ZO	NM	NB
	NM	NM	ZO	PB	ZO	NM
	ZO	ZO	PM	PB	PM	ZO
	PM	NM	ZO	PM	ZO	NM
	PB	NB	NM	ZO	NM	NB

Source: Authors, (2026).

Table 3: Fuzzy control rules table of differential coefficient.

$\Delta \mathbf{K_d}$		$\mathbf{e}(t)$				
		NB	NM	ZO	PM	PB
$\dot{\mathbf{e}}(t)$	NB	PB	PB	NM	PB	PB
	NM	PM	PM	PM	PM	PM
	ZO	NM	ZO	ZO	ZO	NM
	PM	PM	PM	PM	PM	PM
	PB	PB	PB	NM	PB	PB

Source: Authors, (2026).

III.2 PID CONTROLLER

The PID controller is one of the most widely used control strategies in marine applications due to its simple structure, ease of implementation, and satisfactory performance for a wide range of operating conditions [9], [14] . In the case of an ASV, PID control is applied to minimize the tracking errors in surge, sway, and yaw directions [4], with the control law:

$$\mathbf{u}(t) = \mathbf{K_p}\mathbf{e}(t) + \mathbf{K_i}\int_0^t \mathbf{e}(t)dt + \mathbf{K_d}\dot{\mathbf{e}}(t) \tag{15}$$

where $\mathbf{e}(t) = \boldsymbol{\eta}_{\mathbf{ref}}(t) - \boldsymbol{\eta}(t) = [e_x \;\; e_y \;\; e_\psi]^T$ denotes the tracking errors in surge, sway, and yaw directions. The gain matrices $\mathbf{K_p}, \mathbf{K_i}, \mathbf{K_d}$ are diagonal and tuned separately for each degree of freedom, $\mathbf{K_p}, \mathbf{K_i}, \mathbf{K_d} \in \mathbb{R}^3$ are diagonal gain matrices,

$$\mathbf{K_p} = \text{diag}\{K_p^x, K_p^y, K_p^\psi\},\ \mathbf{K_i} = \text{diag}\{K_i^x, K_i^y, K_i^\psi\},\ \mathbf{K_d} = \text{diag}\{K_d^x, K_d^y, K_d^\psi\}$$

IV. RESULTS AND DISCUSSION

IV.1 SIMULATION SETUP

The ASV dynamics follow standard marine-vehicle formulations, comprising rigid-body inertia, added mass, Coriolis/centripetal terms, linear-quadratic hydrodynamic damping, and external disturbances [3].

Table 4: General ship parameters.

Parameter	Value	Description
m	10	ASV mass
I_Z	1.76	Moment of inertia about yaw axis
x_G	0.046	Center of gravity position along x-axis
y_G	0	Center of gravity position along y-axis
T_S	0.01	Sampling time

Source: Authors, (2026).

Table 5: Added mass coefficients.

Parameter	Value	Description
$\dot{X}_u$	−2	Added mass surge
$\dot{Y}_v$	−10	Added mass sway
$\dot{Y}_r$	−0	Added mass sway do yaw
$\dot{N}_v$	−0	Added mass yaw do sway
$\dot{N}_r$	−1	Added mass yaw

Source: Authors, (2026).

Table 6: Hydrodynamic damping coefficients.

Parameter	Value	Description
X_u	–0.72253	Linear surge damping
Y_v	–0.88965	Linear sway damping
Y_r	–7.25	Sway damping due to yaw
N_v	0.3130	Yaw damping due to sway
N_r	–1.9	Yaw damping moment
$X_{u\|u\|}$	–1.32742	Nonlinear surge damping
$Y_{v\|v\|}$	–36.47287	Nonlinear sway damping
$Y_{\|r\|v}$	–0.845	Yaw-sway cross-coupled damping coefficient
$Y_{\|v\|r}$	–0.805	Sway-yaw cross-coupled damping coefficient
$Y_{\|r\|r}$	–3.45	Nonlinear yaw damping
$N_{v\|v\|}$	–3.95645	Yaw moment due to sway
$N_{\|r\|v}$	–0.08	Yaw moment coupling
$N_{\|v\|r}$	0.13	Yaw moment coupling
$N_{\|r\|r}$	–0.75	Nonlinear yaw damping

Source: Authors, (2026).

In this research, two trajectories are employed for simulation and discussion, including circular and lemniscate paths. For the Fuzzy–PID controller, the initial gain matrices are defined in diagonal form to simplify the implementation process. The nominal values of these parameters are summarized in Table 7 below:

Table 7: Initial conditions and nominal controller gains.

Trajectory	$\begin{bmatrix} X_0 & Y_0 & \psi_0 \end{bmatrix}$	$\mathbf{K_p} = diag\{K_p^x, K_p^y, K_p^\psi\}$	$\mathbf{K_i} = diag\{K_i^x, K_i^y, K_i^\psi\}$	$\mathbf{K_d} = diag\{K_d^x, K_d^y, K_d^\psi\}$
Circular	$\begin{bmatrix} 0 & 0 & 0 \end{bmatrix}$	$diag\{100,100,1\}$	$diag\{0,0,1\}$	$diag\{100,100,1\}$
Lemniscate	$\begin{bmatrix} 0 & 0 & 0 \end{bmatrix}$	$diag\{100,100,1\}$	$diag\{2,0,1\}$	$diag\{100,100,1\}$

Source: Authors, (2026).

To evaluate the tracking accuracy objectively and fairly, the RMSE and the IAE are employed. RMSE penalizes large deviations and reflects the overall energy of the error, while IAE measures the accumulated error performance over time.

$$RMSE = \sqrt{\frac{1}{T}\int_0^T e^2(t)\,dt} \tag{16}$$

$$IAE = \int_0^T |e(t)|dt \tag{17}$$

IV.2 SIMULATION RESULT AND DISCUSSION

Figures 5 to 12 present the motion of the ASV and its pose while tracking two reference paths: a circular trajectory and a lemniscate trajectory. The vehicle starts from the initial condition and tracks the reference paths. As shown in the response plots (Figures 6 and 10), error plots (Figures 7 and 11), and control signal plots (Figures 8 and 12), the proposed Fuzzy-PID controller is compared against a conventional PID in terms of tracking accuracy and control effort. Both controllers exhibit transient peaks when the reference changes abruptly, most notably during the initial phase and at the lemniscate crossover. However, the Fuzzy-PID yields smaller error envelopes, smoother control inputs, faster settling times, and effectively eliminates the steady-state bias in the heading observed with the conventional PID. Overall, the Fuzzy-PID achieves tighter path-following and improved robustness under the nonlinear, coupled ASV dynamics.

IV.2.1 Circular Trajectory Result

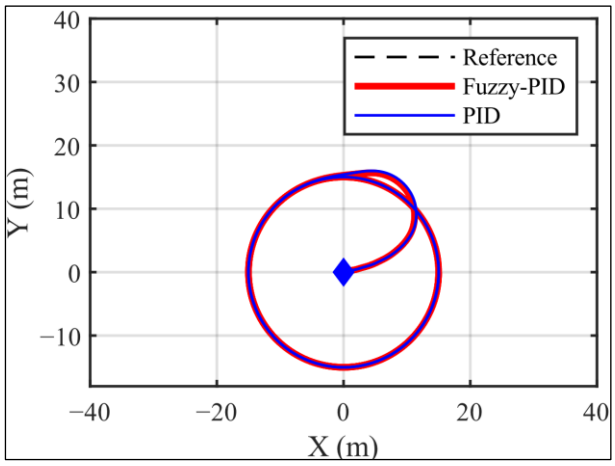

Figure 5: Following path of circular trajectory.
Source: Authors, (2026).

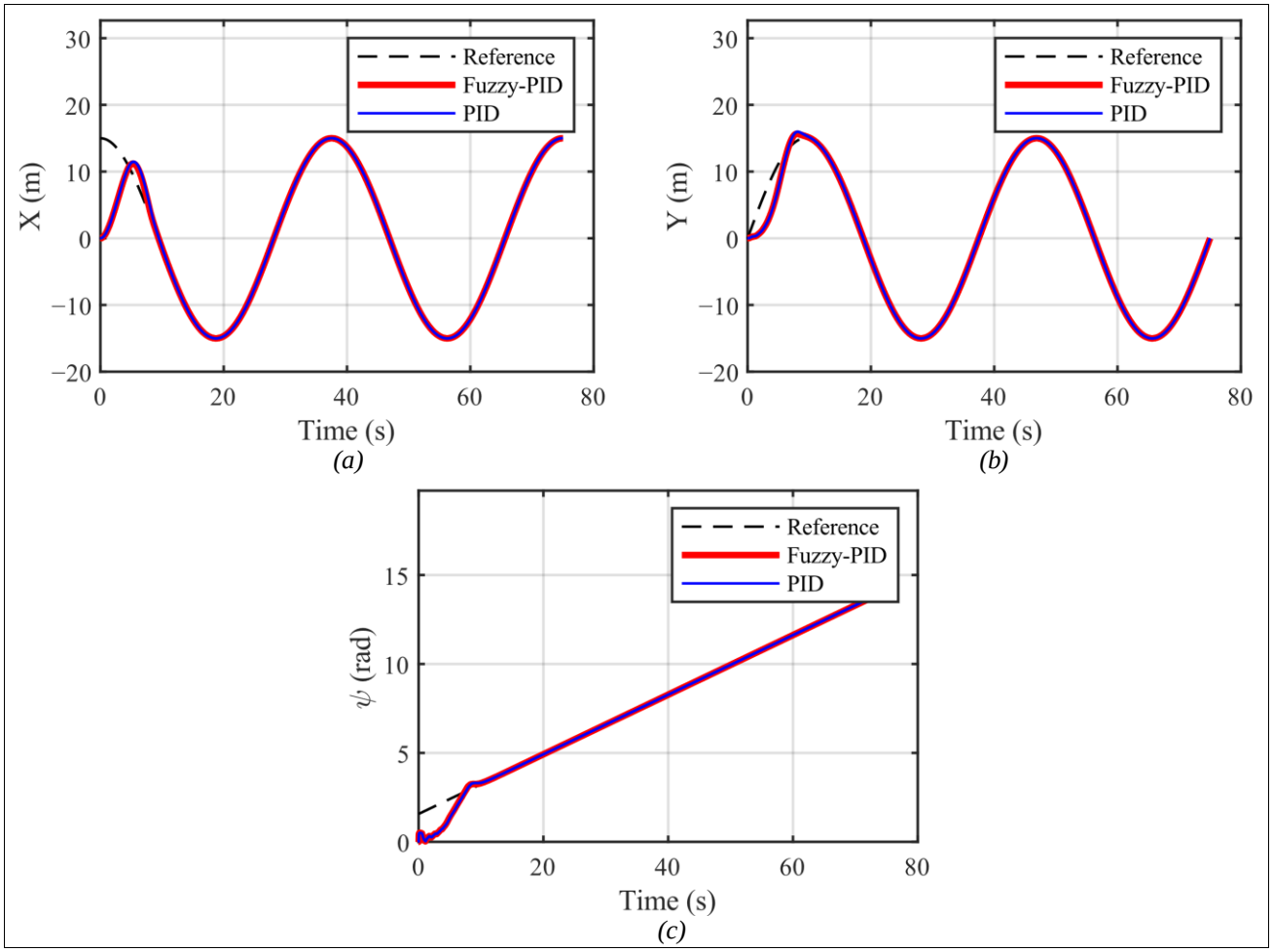

Figure 6: Circular path-following response (a) X-axis, (b) Y-axis, (c) ψ angle.
Source: Authors, (2026).

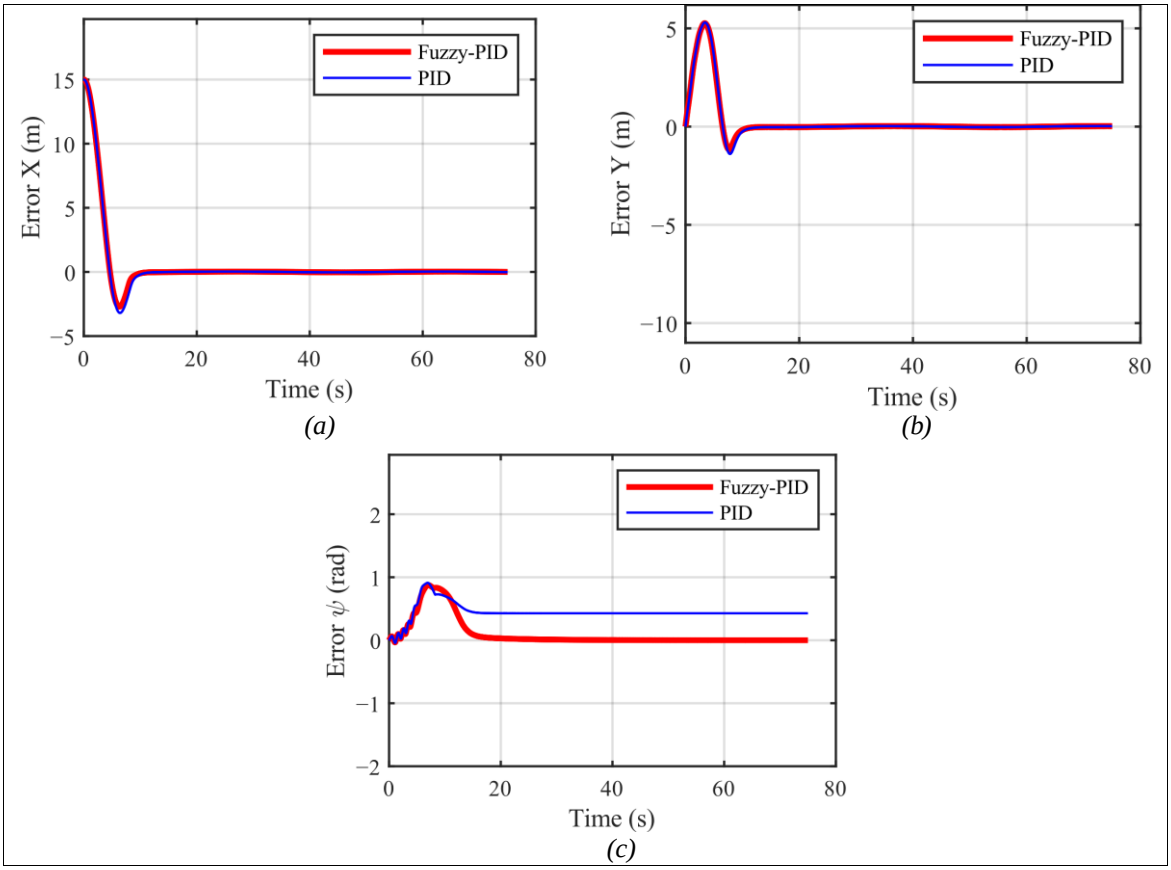

Figure 7: Tracking errors for following a circular trajectory (a) error in X-axis, (b) error in Y-axis and (c) heading error ψ .
Source: Authors, (2026).

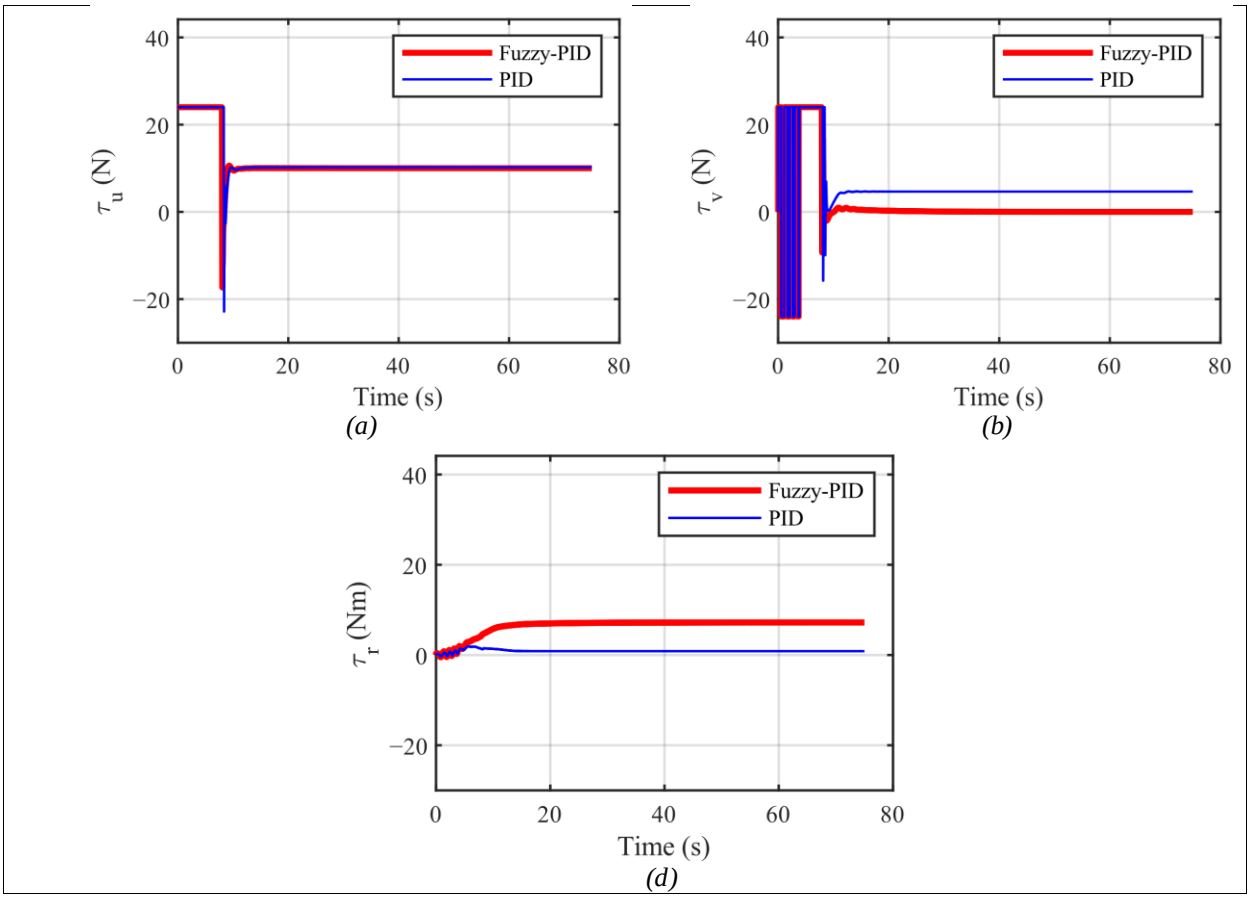

Figure 8: Control signals for following a circular trajectory (a) torque in X-axis, (b) torque in Y-axis and (c) moment around the Z-axis.
Source: Authors, (2026).

Figures 5 and 6 illustrate the position and angle tracking performance for the circular trajectory. While both controllers achieve satisfactory path-following accuracy in the XY-plane, a significant difference emerges in the heading control. As detailed in Figure 7(c), the conventional PID controller maintains a notable steady-state heading offset of approximately 0.5 radian after the initial transient phase. This offset is indicative of the fixed-gain PID's inability to fully adapt to the strong cross-coupling and nonlinearities inherent in the ASV dynamics during continuous rotation. In sharp contrast, the proposed Fuzzy-PID controller successfully eliminates this offset, achieving a faster settling time and converging to near-zero steady-state heading error. The superior adaptability of the Fuzzy-PID, driven by the online gain tuning, results in a visibly smoother overall path (Figure 5) compared to the fixed-gain PID.

The analysis of the control signals in Figure 8 reveals a distinct advantage of the Fuzzy-PID scheme regarding actuator usage. During the initial acceleration phase, the conventional PID controller exhibits severe saturation and high-frequency chattering in the sway force (τ_v) and sharp spikes in the surge force (τ_u). Such aggressive control actions are detrimental to the propulsion system, leading to increased mechanical wear and energy waste. In contrast, the Fuzzy-PID controller synthesizes significantly smoother force profiles with reduced peak amplitudes, effectively mitigating the initial transient shock. Regarding the yaw moment (τ_r), the Fuzzy-PID rapidly settles to the stable equilibrium torque required for the constant-radius turn, whereas the PID signal shows a slower convergence with residual fluctuations, indicating a struggle to counterbalance the coupled sway-yaw hydrodynamics effectively.

IV.2.2 Lemniscate Trajectory Result

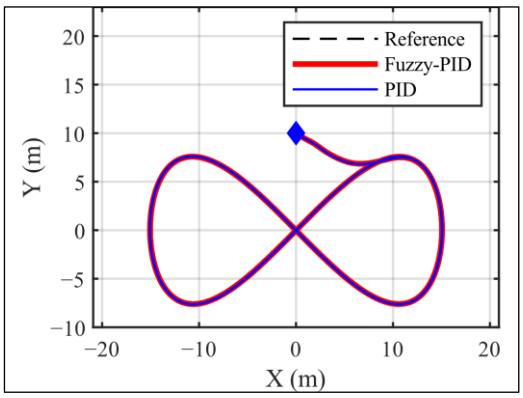

Figure 9: Following path of lemniscate trajectory.
Source: Authors, (2026).

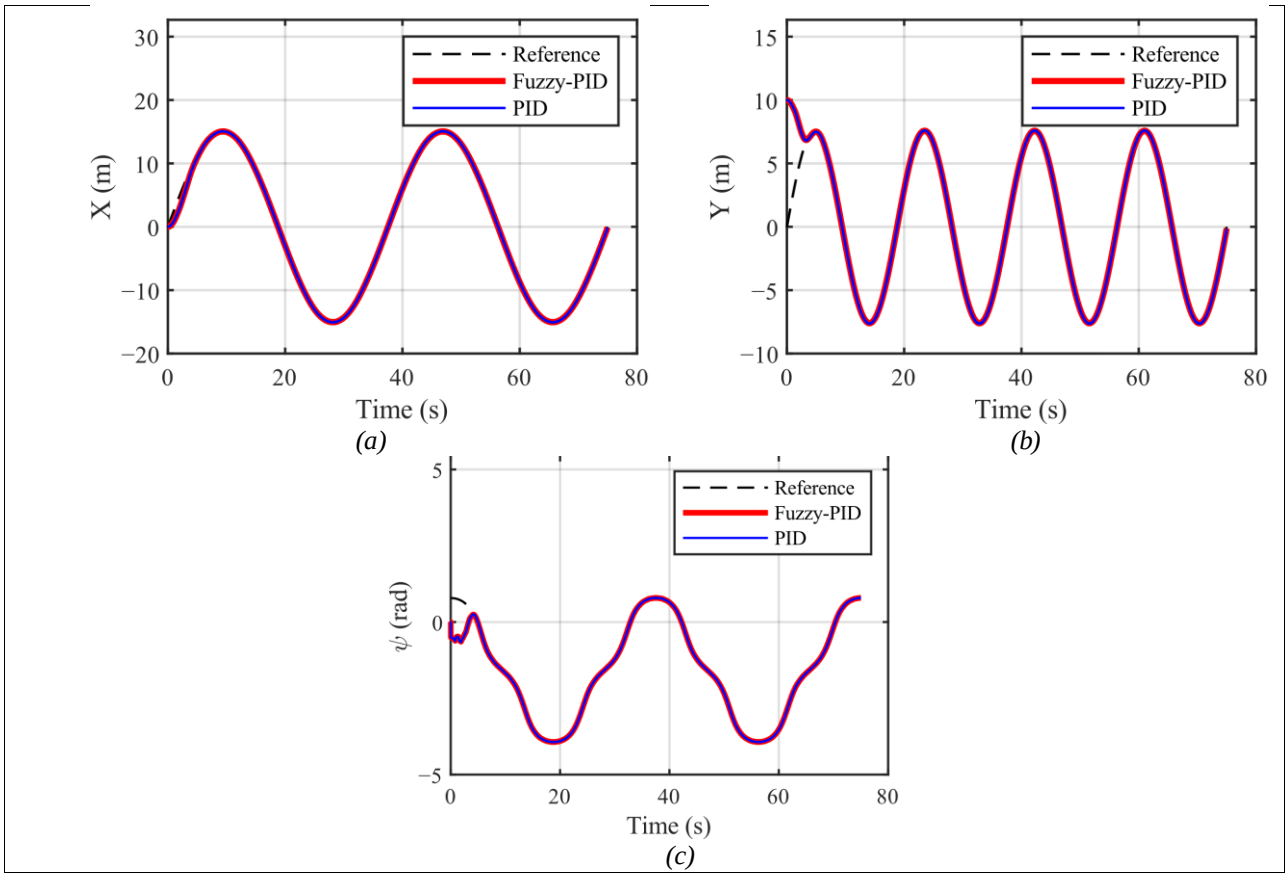

Figure 10: Lemniscate path-following] response (a) X-axis, (b) Y-axis, (c) ψ angle and (d) tracking path.
Source: Authors, (2026).

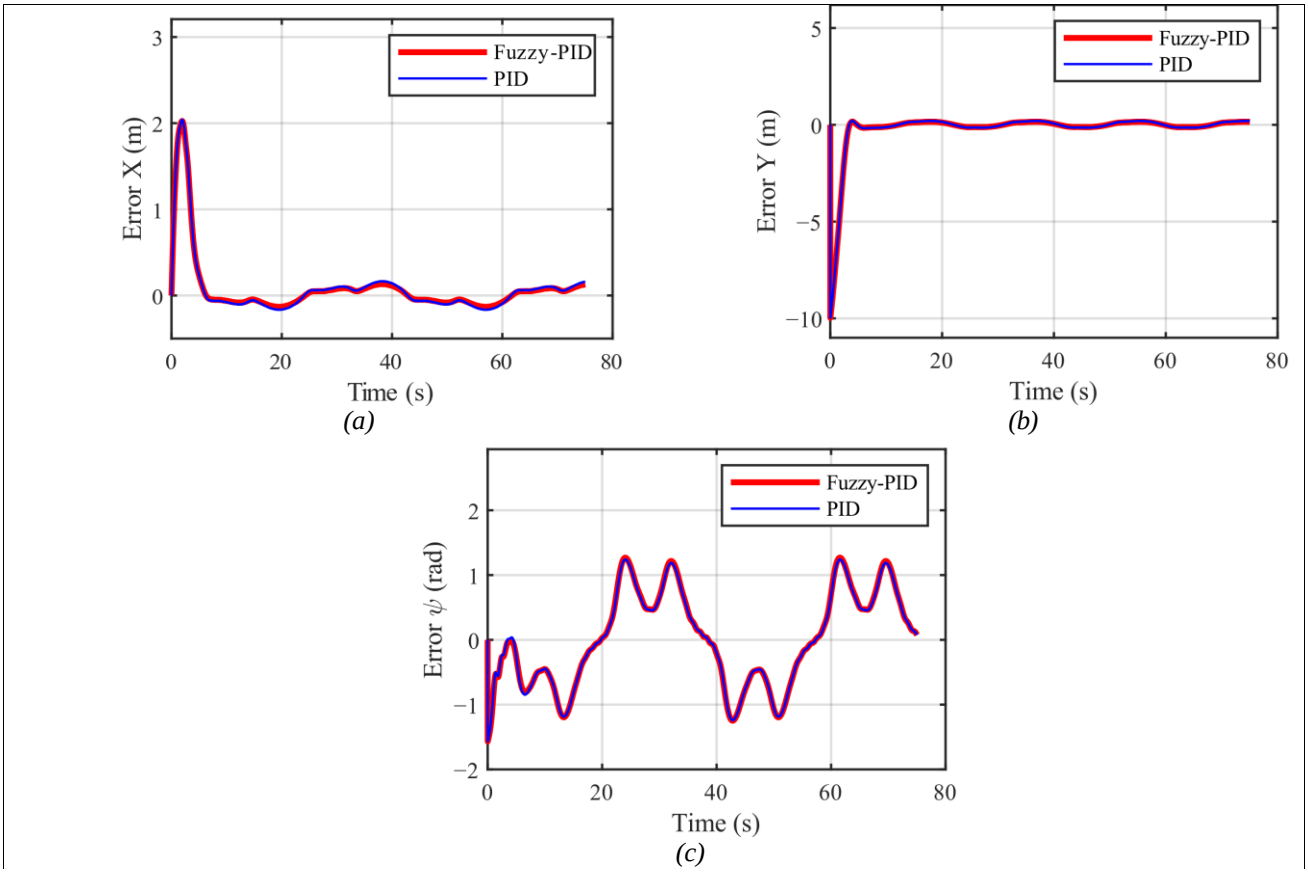

Figure 11: Tracking errors for following a lemniscate trajectory (a) error in X-axis, (b) error in Y-axis and (c) heading error ψ .
Source: Authors, (2026).

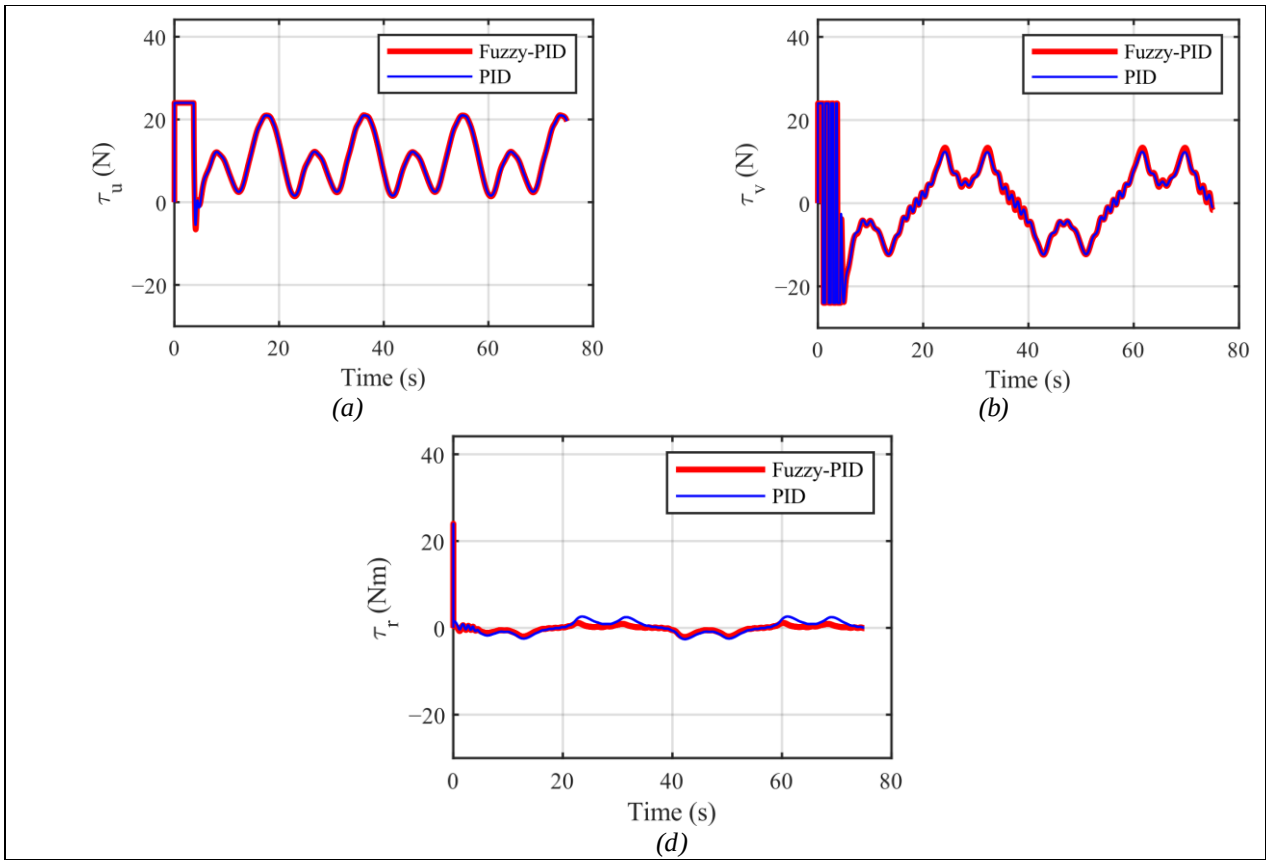

Figure 12: Control signals for following a lemniscate trajectory (a) torque in X-axis, (b) torque in Y-axis and (c) moment around the Z-axis.
Source: Authors, (2025).

The lemniscate trajectory (Figure 9) presents a more demanding scenario, imposing alternating curvature and progressively challenging the surge-sway-yaw coupling. Figure 11, which plots the tracking errors, confirms that the Fuzzy-PID is more effective at handling these dynamic changes. The PID controller exhibits quasi-periodic oscillations in the heading error ψ, synchronized with the reference trajectory's curvature reversals, and occasionally retains a small residual bias after transients. By employing adaptive gain tuning, the Fuzzy-PID controller significantly damps these oscillations faster, reduces the peak-to-peak error, and maintains superior accuracy. As shown in Figure 10, the Fuzzy-PID tracks the path more tightly around high-curvature segments and at the self-intersection point, whereas the PID tends to exhibit greater lag and overshoot. Overall, the fuzzy self-tuning mechanism improves the controller's robustness and adaptability to time-varying path curvature.

For the more complex lemniscate maneuver, the control signal performance presented in Figure 12 further underscores the robustness of the proposed method. The critical challenge in this scenario is the smooth reversal of the yaw moment τ_r at the trajectory's inflection point. The conventional PID controller struggles with this transition, producing a control signal characterized by noticeable ripples and jitter, which suggests that the fixed gains are over-reacting to the rapidly changing curvature and centripetal loads. Conversely, the Fuzzy-PID controller modulates the gains online to generate a clean, continuous torque curve, seamlessly transitioning between turning directions without inducing oscillatory behavior. Furthermore, the surge and sway forces (τ_u, τ_v) under Fuzzy-PID control remain within a tighter envelope compared to the PID, confirming that the adaptive mechanism not only improves tracking accuracy but also yields a more energy-efficient and actuator-friendly control strategy. This table summarizes the performance metrics (RMSE, IAE) for the ASV model under PID and Fuzzy-PID control.

Table 8: RMSE and IAE results of PID and Fuzzy-PID controllers under circular trajectory.

Trajectory	Controller	Axis	RMSE	IAE	Unit
Circular	PID	X	2.616284	53.225904	m
		Y	1.139514	26.534804	m
		ψ	0.564364	40.522358	rad
	Fuzzy -PID	X	2.597192	50.600787	m
		Y	1.119295	25.107095	m
		ψ	0.303748	14.629701	rad

Source: Authors, (2026).

Table 9: RMSE and IAE results of PID and Fuzzy-PID controllers under lemniscate trajectory.

Trajectory	Controller	Axis	RMSE	IAE	Unit
Lemniscate	PID	X	0.286467	10.736777	m
		Y	0.83173	18.315073	m
		ψ	2.598652	70.327672	rad
	Fuzzy-PID	X	0.276233	9.013106	m
		Y	0.827149	15.94486	m
		ψ	2.585115	70.043016	rad

Source: Authors, (2026).

To rigorously assess the tracking precision, the performance metrics defined in equations (16) and (17) were analyzed. Across the circular trajectory (Table 8), the Fuzzy-PID controller delivers the most significant improvement in heading control. Specifically, the heading RMSE computed via Eq. (16) decreases from 0.564 to 0.304 (a 46% reduction), while the IAE calculated via Eq. (17) drops from 40.52 to 14.63 (a 64% reduction). Position tracking in the X and Y axes also exhibits modest improvements in IAE, resulting in a visibly smoother XY path consistent with enhanced rejection of low-frequency disturbances. In the lemniscate trajectory (Table 9), the Fuzzy-PID controller continues to outperform the PID in translational motion, yielding lower RMSE and IAE values for both X and Y axes. The heading error ψ remains comparable to the PID baseline; however, the controller demonstrates greater stability.

Unlike the PID, which suffers from oscillatory behavior due to the continuous curvature changes, the Fuzzy-PID's adaptive gains provide a steadier response. Overall discussion: The simulation results confirm that the proposed Fuzzy-PID architecture consistently enhances translational tracking and minimizes accumulated error. It proves particularly superior in heading regulation during smooth maneuvering (circular path). While the performance on the complex lemniscate path is robust, future refinements could introduce a curvature-aware term into the fuzzy rules or apply gain scheduling based on the desired yaw rate to further optimize handling during sharp heading reversals.

V. CONCLUSIONS

This study examined trajectory-tracking control for an ASV with nonlinear, strongly coupled surge, sway, and yaw dynamics. A conventional fixed-gain PID was compared with a Fuzzy-PID controller within the same single-loop architecture on circular and lemniscate paths. The results are consistent across trajectories: Fuzzy-PID shortens settling time, reduces overshoot, improves path fidelity in the XY plane, and lowers accumulated tracking error, as confirmed by the RMSE and IAE tables. The advantages are most evident on the circular and lemniscate paths, where Fuzzy-PID removes or greatly reduces the steady-state heading bias in ψ that remains after the initial overshoot of PID, producing visibly smoother tracks.

In the complex lemniscate scenario, the proposed controller effectively manages the dynamic coupling during the direction reversal at the crossover point, avoiding the oscillatory behavior observed with the PID. Furthermore, control signals generated by the Fuzzy-PID are significantly smoother, which implies reduced actuator wear compared with the chattering observed in PID commands under strong coupling. The study intentionally kept a compact rule base and did not carry out exhaustive tuning of membership parameters, leaving scope to further improve robustness and repeatability. Future work will include systematic gain scheduling and parameter optimization across operating points, integration of state and disturbance estimation to suppress wave frequency content and reject slowly varying biases, coordination with energy-aware thrust allocation to respect power limits while maintaining tracking quality, and validation through hardware-in-the-loop tests and field trials under real wind, wave, and current conditions.

VI. AUTHOR'S CONTRIBUTION

Conceptualization and Methodology: Thien M. Tran.
Investigation and Discussion of results: Thien M. Tran and Tien V. Tran.
Writing – Original Draft: Tien V. Tran.
Writing – Review and Editing: Thien M. Tran and Tien V. Tran.
Resources: Tien V. Tran.
Supervision and Corresponding author: Thien M. Tran.
Approval of the final text: Thien M. Tran and Tien V. Tran.

VII. ACKNOWLEDGMENTS

The authors are indebted to Editor board, anonymous reviewers, and HCM-UTE for encouraging comments, suggestions, and conditions which have enhanced the quality of the research paper.

VIII. REFERENCES

[1] A. J. Sørensen, Marine Control Systems: Propulsion and Motion Control of Ships and Ocean Structures. Trondheim, Norway: Dept. of Marine Technology, NTNU, 2013. [Online]. Available: https://assor.folk.ntnu.no/publications/marcyb.pdf

[2] T. M. Tran, "A novel model-free control technique for angular motion of single ducted-fan unmanned aerial vehicle," J. Autom. Mob. Robot. Intell. Syst., vol. 19, no. 2, pp. 34–40, 2025, doi: 10.14313/jamris-2025-012.

[3] T. I. Fossen, Marine Control Systems: Guidance, Navigation and Control of Ships, Rigs and Underwater Vehicles. Trondheim, Norway: Marine Cybernetics, 2002.

[4] S. Zhang, S. Yang, and X. Xiang, "Formation control of autonomous surface vehicle and experimental validation," IFAC-Pap., vol. 52, no. 24, pp. 278–282, 2019, doi: 10.1016/j.ifacol.2019.12.421.

[5] R. Skjetne, Ø. N. Smogeli, and T. I. Fossen, "A nonlinear ship manoeuvering model: Identification and adaptive control with experiments for a model ship," Model. Identif. Control, vol. 25, no. 1, pp. 3–27, 2004, doi: 10.4173/mic.2004.1.1.

[6] W.-Y. Gan, D.-Q. Zhu, W.-L. Xu, and B. Sun, "Survey of trajectory tracking control of autonomous underwater vehicles," J. Mar. Sci. Technol., vol. 25, no. 6, 2017, doi: 10.6119/JMST-017-1226-13.

[7] T. Morel, L. Orihuela, C. Combastel, and G. Bejarano, "Practical identification approach for the actuation dynamics of autonomous surface vehicles with minimal instrumentation," Ocean Eng., vol. 319, p. 120098, Mar. 2025, doi: 10.1016/j.oceaneng.2024.120098.

[8] M. F. dos Santos, A. F. D. S. Neto, L. D. M. Honório, M. F. da Silva, and P. Mercorelli, "Robust and optimal control designed for autonomous surface vessel prototypes," IEEE Access, vol. 11, pp. 9597–9612, 2023, doi: 10.1109/ACCESS.2023.3239591.

[9] K. Kobatake, T. Okazaki, and M. Arima, "Study on optimal tuning of PID autopilot for autonomous surface vehicle," IFAC-PapersOnLine, vol. 52, no. 21, pp. 335–340, 2019, doi: 10.1016/j.ifacol.2019.12.329.

[10] R. Katebi and Q. Saeed, "Nonlinear predictive PID control design for ship manoeuvering," IFAC Proc. Vol., vol. 42, no. 18, pp. 86–90, 2009, doi: 10.3182/20090901-3-US-2007.00015.

[11] G. Lyu, Z. Peng, and J. Wang, "Safety-certified parallel model predictive control of autonomous surface vehicles via neurodynamic optimization," IEEECAA J. Autom. Sin., vol. 12, no. 10, pp. 2056–2066, 2025, doi: 10.1109/JAS.2024.124980.

[12] H. T. Shandiz, M. E. Hajipour, and A. A. Bagheri, "Position tracking control of ASV based on dynamic inversion with intelligent methods," J. AI Data Min., vol. 12, no. 2, pp. 227–240, 2024, doi: 10.22044/jadm.2024.14081.2516.

[13] D. P. Riananda, N. H. Cahyadi, Z. M. A. Putra, J. Endrasmono, R. Y. Adhitya, and A. Khumaidi, "Orientation Holding Control for Autonomous Surface Vehicles using Adaptive Neuro-Fuzzy Inference System Method," in International Conference on Maritime Technology and Its Application (ICOMTA), Jan. 2025, pp. 13–21. doi: 10.35991/Icomta.v1i1.2.

[14] J. Crowe et al., PID Control: New Identification and Design Methods. London, U.K.: Springer-Verlag, 2005.

[15] J. H. Lilly, Fuzzy Control and Identification. Hoboken, NJ, USA: John Wiley & Sons, 2011.

[16] Y. Bai and D. Wang, "Fundamentals of fuzzy logic control–fuzzy sets, fuzzy rules and defuzzifications," in Advanced Fuzzy Logic Technologies in Industrial Applications, Y. Bai, H. Zhuang, and D. Wang, Eds., London, U.K.: Springer, 2006, pp. 17–36. doi: 10.1007/978-1-84628-469-4_2.